GROUP 4: RECENT APPLICATIONS AND RESULTS OF DIFFRACTION STUDIES

Acta Cryst. (1995). B**51**, 547–558

Structural–Electronic Relationships in Rutile

BY JEREMY K. BURDETT

Department of Chemistry and James Franck Institute, The University of Chicago, Chicago, IL 60637, USA

(*Received* 2 *August* 1994; *accepted* 28 *November* 1994)

Abstract

Several structural details of the rutile family of compounds are examined which highlight the power of orbital models of electronic structure. They include discussion of the local distortion of the octahedron as a function of electron count, distortions driven by metal–metal bonding, and the factors controlling the planar geometry at oxygen.

Introduction

One of my aims at this symposium was to give a sense of how a focused study of the results of electronic structure calculations can lead to a real feel for the factors determining the geometrical structure of a solid as determined by the crystallographer. For this purpose I have chosen, largely from our own studies, a deceptively simple example, that of rutile. We will see that there is a rich variety of connections between the electronic and geometrical structure which are useful illustrators of these approaches in solid-state chemistry in general.

The rutile structure itself is shown from several viewpoints in Fig. 1. It contains metal atoms in octahedral coordination and nonmetal in planar three-coordination. Notice that one of these stresses its derivation from a hexagonal close-packed array of oxide ions with the Ti atoms occupying half the octahedral holes. The rutile structure has received a large amount of attention from Baur (1981), and he has pointed out that it is in fact quite distorted from such a hexagonal close packing and has described it in terms of a tetragonal close packing. Other views [Fig. 1(*c*)] highlight the framework nature of the structure, the planar coordination of oxygen by three metal atoms and the chains [Fig. 1(*d*)] of edge-sharing octahedral which run through the structure. For what combinations of elements is the rutile structure found? One useful way of providing a general answer to this question is to find a pair of indices, ξ_A, ξ_X, for A and X which when plotted for a database of known structures leads to regions which separate one structure from another. The indices may be electronegativity or ionic radius, but one useful index is the pseudopotential radius, a quantum mechanical derived quantity (Cohen, 1981; Zunger, 1981) which is independent of crystal structure or coordination number. Fig. 2 shows such a structure map (Burdett, Price & Price, 1981) for some AX_2 systems, and as may be seen the rutile structure is the one usually found for small anions, X, namely for metal oxides and fluorides. For the chalcogenides and heavier halides it is one of the cadmium halide or molybdenum sulfide polytypes which are found. (The cadmium chloride structure is shown in Fig. 3. Notice it contains pyramidal three-coordinate nonmetals and octahedral metal coordination.) There are exceptions to this general rule. For example, PtO_2 is found in the $CaCl_2$ structure (Rogers, Shannon, Sleight & Gilson, 1969).

There are several distorted relatives of rutile which are relevant to our discussion below and these are shown in Fig. 4. The 'ideal' structure with six equal $A—X$ distances in the AX_6 octahedron is not required by symmetry in the space group $P4_2/mmm$, but the local geometry is one where the AX distances fall into two sets, four equal distances (r_4) involved in edge-sharing in the chain of Fig. 1(*d*), and two (r_2) perpendicular to them. There are thus two types of tetragonal structure, (**1**) with $r_2/r_4 > 1$ (this two long–four short structure is found for TiO_2 itself) and (**2**) with $r_2/r_4 < 1$ (this two short–four long structure is found for FeF_2, for example). A related

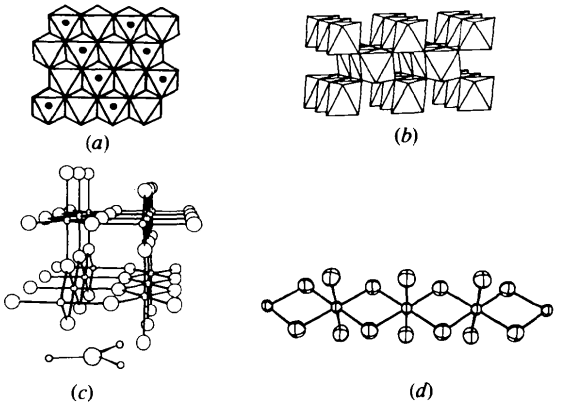

Fig. 1. The rutile structure from several viewpoints. (*a*) Its derivation from a hexagonal close-packed array of anions by filling half the octahedral holes. (*b*) The connectivity of the resulting metal-centered octahedra. (*c*) A ball-and-stick framework diagram highlighting the planar three-coordination of the anion in the inset picture. (*d*) The chains of edge-sharing octahedra characteristic of this structure.

distorted structure (**1***) is where there are three *trans* pairs of equal $A—X$ distances with one pair in the chain of Fig. 1(*d*) being considerably longer than the other two. This monoclinic two long–four short structure is found for the classic Jahn–Teller system CuF_2. Of interest to us later is the observation that in the rutile structure the anion is coordinated by metal in a rigorously planar environment. In the orthorhombic $CaCl_2$ structure (3), the anion is now pyramidal. In several transition metal oxides the metal atoms dimerize as in Fig. 5(*a*) to give the MoO_2 structure (**4**). Sometimes, whether the rutile or MoO_2 structure is adopted is temperature-dependent. For example, VO_2 has the MoO_2 structure below 340 K and the rutile structure above this temperature (Rogers, Shannon, Sleight & Gilson, 1989). For some systems, *e.g.* α-PbO_2, the structure adopted has zigzag rather than linear chains [Fig. 5(*b*)]. Some other interesting rutile derivative structures have been discussed by Baur (1994).

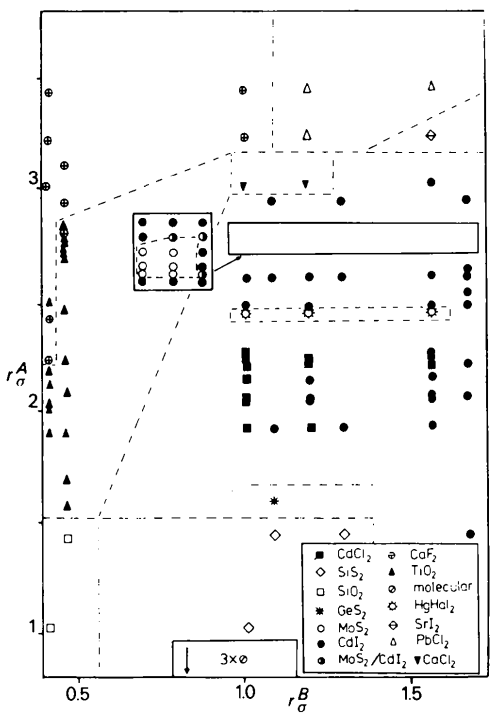

Fig. 2. A structure map for some AX_2 systems. For a database of AX_2 solids a plot of a set of pairs of indices, ξ_A, ξ_X, for A and X for known structures leads to regions where only one structure type is found or predominates. The indices in this plot are pseudopotential radii.

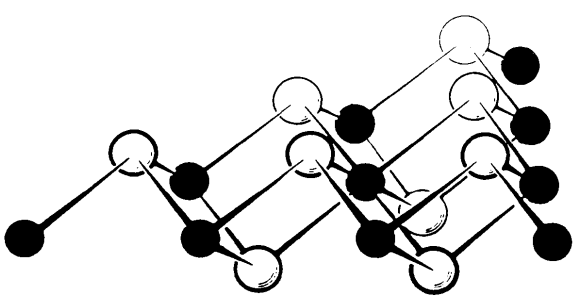

Fig. 3. The cadmium chloride structure. Note that although it contains octahedral six-coordinate cations and three-coordinate anions, just as in rutile, the latter are in a pyramidal geometry.

'Old' theory

Since the rutile structure is found for fluorides and oxides, it is not at all surprising that the simplest model used to describe it is ionic, and that some of the distortions of the structure have been traditionally viewed using Crystal Field Theory (Dunn, McClure & Pearson, 1965). First let us consider the ionic model. Much of the inorganic crystal chemistry of 'ionic' compounds is described in terms of 'close-packed' arrangements, of anions usually, in which ions of the opposite type occupy holes in the structure (Evans, 1964). However, such a model has come under attack over the years. For

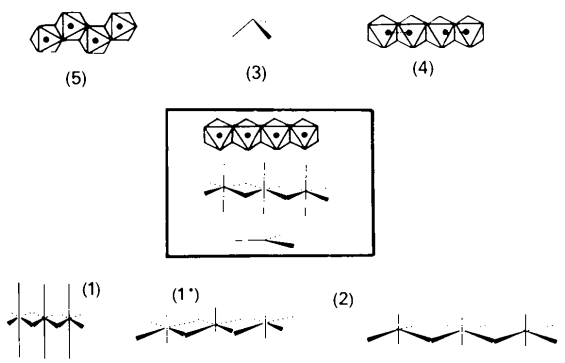

Fig. 4. Rutile relatives: (**1**) tetragonal with $r_2/r_4 > 1$, (**2**) tetragonal with $r_2/r_4 < 1$ and (**1***) monoclinic with $r_2/r_4 > 1$. Here there are three *trans* pairs of equal A–X distances, with one pair in the chain being considerably longer than the other two. The distortions are exaggerated for effect. (**3**) The orthorhombic $CaCl_2$ structure, (**4**) the MoO_2 structure with pairs of metal atoms and (**5**) the α-PbO_2 structure.

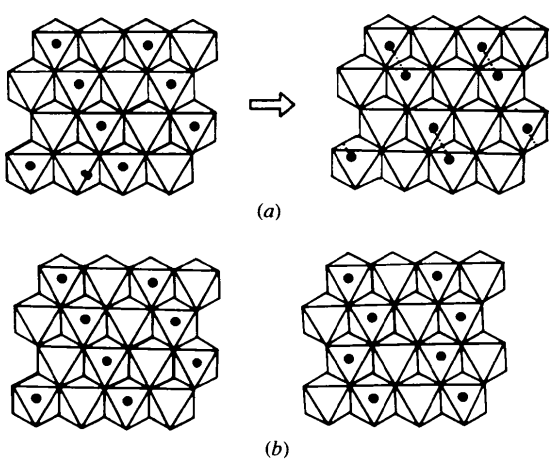

Fig. 5. (*a*) The relationship between the rutile and MoO_2 structures showing the pairing up of the metal atoms. (*b*) The α-PbO_2 structure showing the zigzag chains.

example, because of their mutual electrostatic repulsion a collection of like-charged particles are not likely to 'pack' together at all. In fact, O'Keeffe (1977) has suggested that the details of the structure of the solid are determined by minimizing these repulsive anion–anion (irrespective of their ionic or orbital nature) contacts for a fixed anion–cation distance. The most stable structure is, therefore, expected to be the one of *maximum* anion volume rather than the *minimum* anion volume expected for close-packing. We can use this idea to study the rutile and $CaCl_2$ structures.

The $CaCl_2$ structure is orthorhombic (*Pnnm*) with the cations in 2(*a*) (0,0,0) and $(\frac{1}{2},\frac{1}{2},\frac{1}{2})$ and the anions in 4(*g*) $\pm(u,v,0)$, $\pm(u+\frac{3}{2},\frac{1}{2}-v,\frac{1}{2})$. If $a=b$ and $u=v$, the tetragonal rutile structure results. The parameters of this structure are thus $u, v, \zeta = b/a$ and $\eta = c/a$. Assuming that the six anion–cation distances are equal (l)

$$\zeta^2 = 4u + 4v\eta^2 - 1 - \eta^2, \qquad (1)$$

and the volume with this restriction becomes

$$V^2 = l^6\eta^2(4u + 4\eta^2 v - 1 - \eta^2)/(u^2 + \eta^2 v^2)^3, \qquad (2)$$

it is a trivial matter to maximize V. This is for $u = v = 0.300$, $\eta = 1$, $\zeta = (2/5)^{1/2} = 0.632$. Rutile itself has $u = 0.305$, $\zeta = 0.634$ and, since it is tetragonal, $\eta = 1$. This structure is geometrically a long way away from the 'close-packed' array, which corresponds to $u = 0.289$, $v = 0.25$, $\eta = 0.816$ and $\zeta = 0.6$, and close to that calculated on this simple model. Thus, the importance of *repulsive* anion–anion interactions in setting structural details is clear. This viewpoint will be developed further throughout the article.

One of the first theoretical studies on rutile was by Pauling (1929), who found that only by inclusion of a Born-type repulsion [see (3)] between the O atoms of the chains [Fig. 1(*d*)], in addition to the Coulombic one, could he reproduce the broad details of the structure. Without such a term these chains collapsed, such that the O–O distance perpendicular to the chain (the shared octahedral edge) was far too short. Baur (1961) found that by using a Lennard–Jones potential to supplement the Madelung term he could obtain values of $u = 0.306$ and $c/a = 0.644$ (*cf.* with Table 1). Clearly the bare ionic model is inadequate; other terms need to be added. More insights into the ionic model come from studies (Burdett, 1988*b*; Smyth, unpublished) on the rutile structure using a Born–Mayer potential with the addition of a van der Waals attraction.

$$\Phi(r_{ij}) = q_i q_j / r_{ij} + B_{ij}\exp(-r_{ij}/\rho_{ij}) - C_{ij}/r_{ij}^6 \qquad (3)$$

The total energy is the sum of the terms of (3) over all atom pairs in the solid. The first term is attractive for unlike ions and repulsive for like ions and just becomes the Madelung sum. B_{ij}, ρ_{ij} and C_{ij} are adjustable parameters and are determined (Catlow & Mackrodt, 1982) by fitting to an experimentally observed structure.

Table 1. *Calculated dimensions of the rutile structure (distances in* Å)

	Observed	Madelung, plus Ti–O repulsion	Calculated Madelung plus Ti–O and O–O potentials	Ti–O and O–O potentials,* zero Ti, O charges
a	4.587	4.246	4.593	4.567
c	2.959	3.429	2.958	2.957
c/*a*	0.645	0.808	0.644	0.647
u†	0.305	0.309	0.305	0.302

* Adjusted to fit the structure.
† Oxygen *z* coordinate.

Table 1 shows some results. The second column gives the observed dimensions of rutile. The third column shows the poor agreement found if O–O interactions are left out of the calculation, a result similar to the results of Pauling and Baur described above. The third column shows the results of a full calculation with all Ti–Ti, Ti–O and O–O interactions included. In the lead term of (3), the charge on Ti was 4+ and on O 2−. In the last column the results are just as good, but were computed with charges on Ti and O of zero! Thus, although the results of the calculations fit the experiment, there is clearly no confirmation that the system is 'ionic'. Although (3) is a good mimic of the experiment, its failure to distinguish between Ti^{4+} and Ti^{0+} is at first sight embarrassing. However, although such studies using the potential of (3) imply an ionic model, it should be realized that over the range of internuclear distances sampled in many structural problems, other potentials may be equally as good, as long as they adequately represent the attractive and repulsive parts of the potential. Thus, just because an 'ionic' model is used, this does not demand an 'ionic' description of the chemical bonding.

Although the Baur (1961) calculations noted above reproduce u and c/a reasonably well, they do in fact fail when it comes to predicting the direction of the distortion of the octahedron away from its regular geometry (Baur, 1976; Baur & Khan, 1971). These calculations predict a distortion of the form (**2**), whereas the observed distortion for TiO_2 is (**1**).

Table 2 gives some structural data for these rutile oxides and fluorides. As noted earlier, (**1***) structures of CuF_2 and CrF_2 are textbook examples of Jahn–Teller distorted systems. [The Jahn–Teller theorem (Jahn & Teller, 1937) will be discussed in detail below.] Fig. 6(*a*) shows how the e_g orbitals of an octahedrally coordinated transition metal ion are expected to change as a result of a two long–four short distortion or a two short–four long distortion. Although traditionally this picture was constructed using the Crystal Field Model (Dunn, McClure & Pearson, 1965), an orbital approach gives the same qualitative picture. Notice the removal of the degeneracy of the e_g levels and the clear stabilization of the d^9 and high-spin (h.s.) d^4 configurations on distortion. Fig. 6(*b*) shows the splitting pattern for the t_{2g} levels for the two long–four short distortion. Again Crystal Field argu-

ments are traditionally used, but the same qualitative result is found if π-donor ligands are used. This picture would also apply to the local geometry preferences of the solid assuming a localized electronic picture. Whereas for e_g degeneracies the model as shown leads to no predictions as to the sense (**1** or **2**) of the distortion, it does make predictions as to their sense for t_{2g}

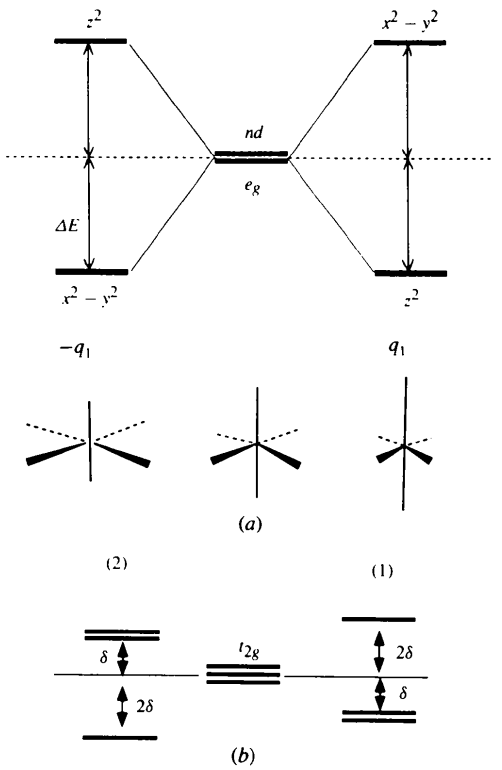

Fig. 6. Energy changes expected for the (*a*) e_g and (*b*) t_{2g} orbitals of an octahedrally coordinated transition metal ion on distortion.

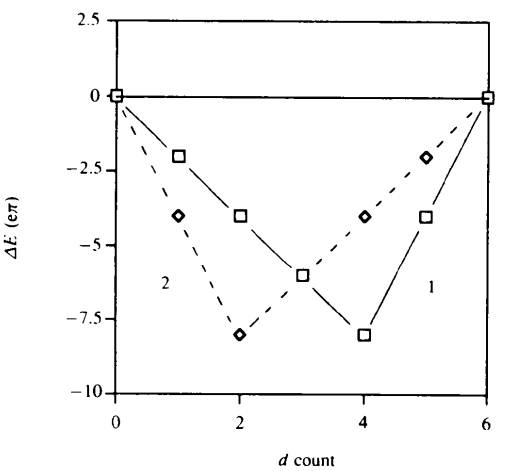

Fig. 7. The stabilization energy on distortion away from octahedral for the two long–four short (**1**) or two short—four long (**2**) pathway for low-spin systems d^0–d^6, using the model of Fig. 6 and calculated using the Angular Overlap Model.

Table 2. *Bond length ratios in rutile fluorides and oxides*

		d count	$(1 - r_4/r_2) \times 100$	Type	Local model	Extended model
Fluorides	Mg	0	0.96	2	–	–
	Cr	h.s. 4	−17.7	1*	–	–
	Mn	h.s. 5	1.28	2	–	2
	Fe	h.s. 6	6.01	2	2	2
	Co	h.s. 7	1.09	3	1	2
	Ni	h.s. 8	2.07	2	–	2
	Cu	9	−15.0	1*	–	–
	Zn	10	1.69	2		2
Oxides	Ti	0	−2.06	1	–	1
	Cr	h.s. 2	1.22	2	1	2
	Ru	l.s. 4	2.16	2	1	2
	Os	l.s. 4	2.24	2	1	2

degeneracies. For example a d^1 system is clearly better stabilized by (**2**) (2δ) than (**1**) (δ). These predictions for low-spin systems are shown in Fig. 7. Table 2 shows the predictions (Burdett, Miller, Richardson & Smith, 1985) of this local model for a series of oxides and fluorides. Notice that it is in quite poor agreement with experiment.

'New' theory

Developments in the orbital picture over the past 30 years have revolutionized much of molecular chemistry and in the past 15 years much of solid-state chemistry. The LCAO model has been a powerful scheme with which to provide a unifying basis for many different parts of chemistry (Albright, Burdett & Whangbo, 1985). Molecular chemists are by and large quite happy with a delocalized orbital picture to view 'electron-deficient' molecules, such as the boranes and related metal-containing clusters. Organometallic molecules typified by ferrocene require such electronic descriptions, as do more sophisticated aspects of organic molecules traditionally described by two center–two electron bonds. The quintessential 'delocalized' organic example is the π-system of benzene of course. These delocalized molecular orbitals (MO's) of the molecule are replaced by the delocalized crystal orbitals (CO's) in the solid. Just as the delocalized picture may often be recast as a set of localized two center–two electron bonds (in methane, for example), so may this delocalized solid-state picture often be recast similarly (in diamond, for example). In many, perhaps most cases, however, the delocalized picture is the best one to use.

We will start with molecules. Fig. 8 shows ways of depicting collections of energy levels (Burdett, 1995; Hoffmann, 1988). In the molecular case there are a finite number of levels which are usually depicted, as in Fig. 8(*a*). The example used here employs the π-energy levels of borazine, $B_3N_3H_6$. Figs. 8(*b*) and (*c*) show two constructs which are seldom used in molecular chemistry, but will be useful in examining orbital structure in solids. One is the density-of-states representation of the energy level collection. A line is drawn whose length is proportional to the number of energy levels at a given energy. Examine the construction of Fig. 8(*b*) from the

details of 8(*a*). The second is a projected density of states, where the length of the line is proportional to the boron or nitrogen character of each level. Note that the form of this picture is that expected from the electronegatives of the two atoms. From Mulliken's definition, electronegativity scales with ionization energy. The description of the molecular orbitals are then consistent with the relative energies of the atomic orbitals, boron 2*p* being less strongly bound than nitrogen 2*p*. The deeper-lying orbitals will have a larger contribution from the more electronegative atom (in this case, N). Thus, the length of the lines corresponding to the bonding orbitals in the DOS(N) plot are greater than for their antibonding counterparts. The converse is true for DOS(B). Here the larger B orbital character lies with the least strongly bound levels.

Exactly analogous pictures apply to the solid state, but here there is an infinite collection of orbitals and thus the constructs just described are continuous, applicable to a distribution of energy levels. Atomic energy levels broaden into collections of levels (bands) as in Figs. 9(*a*) and (*b*). These bands may be labeled with their atomic origin, and their relative energies commensurate with their relative ionization energies just as in borazine. Thus, the oxygen 2*s* band for TiO_2 lies deeper in energy than the oxygen 2*p* band. We refer the reader elsewhere (Burdett, 1984, 1995) as to how the actual calculations are done in the solid-state case, but proceed immediately to rutile, our title compound. The energy density of states calculated (Burdett, 1985) for rutile, TiO_2, is shown in Fig. 10(*b*). This may be understood *via* the scheme of Fig. 10(*a*). Bands develop in the energy regions appropriate for the ionization energies of metal and oxygen levels. TiO_2 (d^0) has a gap between filled and empty bands (3.0 eV from experiment). Accordingly, rutile (when pure and stoichiometric) is colorless and an insulator. There are two types of *d* orbital, as a result of the octahedral metal coordination. There is also an energy gap between these e_g and t_{2g} bands. The addition of a few electrons to rutile, however, by exposure to a lithium alkyl turns rutile black and into a metallic

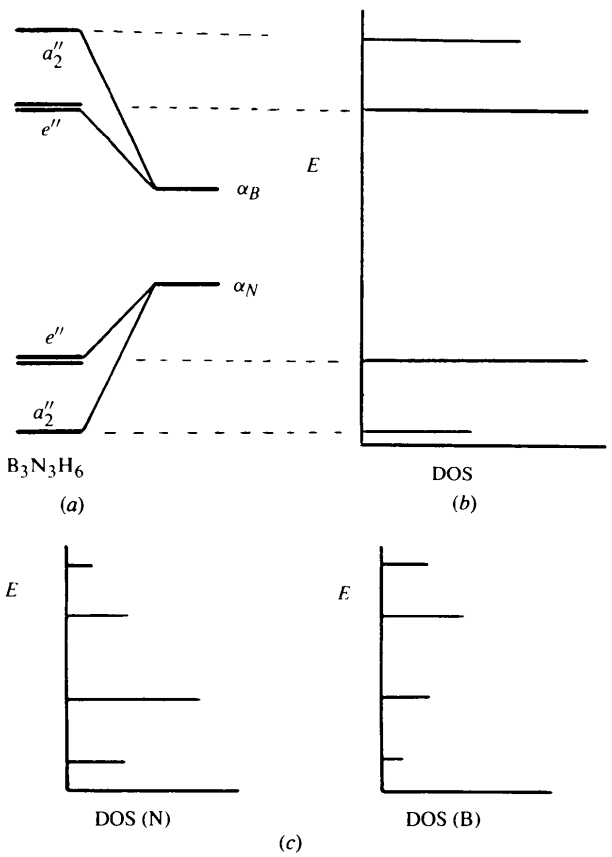

Fig. 8. Orbital tools useful in the study of solids. (*a*) Molecular orbitals for borazine, $B_3N_3H_6$; (*b*) a density-of-states representation of the energy-level collection; (*c*) projected density-of-states for the nitrogen and boron levels.

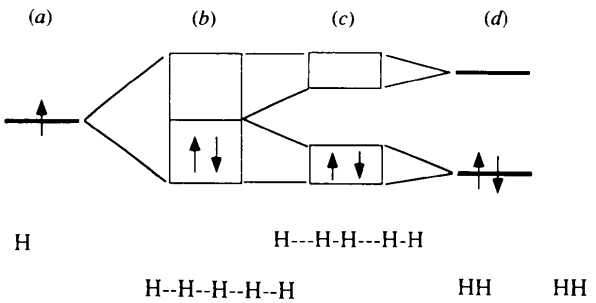

Fig. 9. The Peierls distortion in hydrogen: (*a*) An atomic H 1*s* level; (*b*) the energy band corresponding to a one-dimensional chain of regularly spaced H atoms; (*c*) splitting of the band into two as the chain distorts to alternating short and long H–H distances; (*d*) the extreme case of (*c*) where there are just H–H dimers (*i.e.* H_2 molecules).

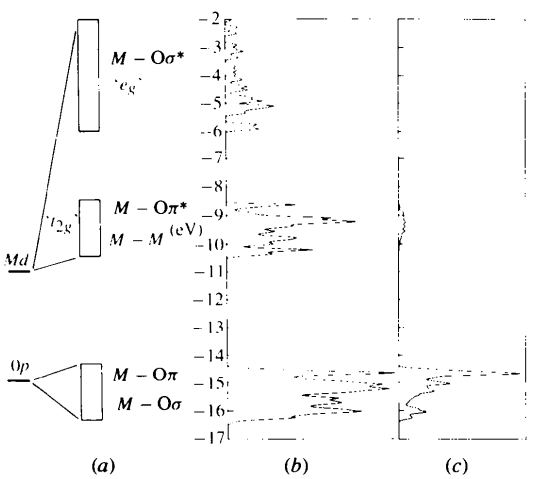

Fig. 10. (*a*) Energies of atomic Ti 3*d* and O 2*p* levels and the bands expected from them in TiO_2. (*b*) The energy density-of-states calculated for rutile TiO_2. This may be understood *via* the scheme of Fig. 9(*a*). (*c*) The projection of the oxygen p_z orbital which lies perpendicular to the OTi_3 plane. All bands below 14 eV are occupied for TiO_2.

conductor. Such a result tells us that the metal t_{2g} band is quite wide. A band partially filled with electrons gives rise to metallic conduction. Fig. 10(*b*) shows that the t_{2g} band derives its width from both *M*–*M* and *M*–O π-interactions. The projection of the oxygen p_z orbital, which lies perpendicular to the OTi_3 plane (inset to Fig. 1*c*) and is involved purely in Ti–O π-interactions, is shown (Burdett, 1985) in the second panel of Fig. 10(*b*) and is quite wide. The properties of the t_{2g} band are particularly important in the study of the MoO_2 structure [Fig. 5(*a*)]. This is found for VO_2, MoO_2, WO_2, α-ReO_2 and TcO_2. NbO_2 has a related but more complex arrangement.

We have noted the possibility of metallic behavior in these materials traditionally regarded as being 'ionic'. This at first sight is unusual, as was recognized many years ago by Goodenough (1965) who suggested that if direct *d*–*d* overlap or metal *d* anion *s* or *p* interaction was large enough, metallic behavior could result.

The $TiO_2 \rightarrow MoO_2$ distortion

The effect on the calculated density of states of the distortion from the basic rutile structure $TiO_2 \rightarrow MoO_2$ [where the metal atoms pair up along the edge-sharing octahedral chains of the parent (Fig. 5(*a*)] is shown (Burdett, 1985) in Fig. 11(*a*). There is a substantially wider band than found in the undistorted parent. Its origin is simply revealed by using one of the techniques described above. Fig. 11(*b*) shows the decomposition of the total density of states into those which are of σ-, π- and δ-symmetry with respect to the edge-sharing chains. Notice the way the σ- and π-components split into two on distortion. This behavior is typical of a Peierls distortion (Peierls, 1955; Burdett, 1995; Hoffmann, 1988). Consider the simplest case, that of a one-dimensional chain of regularly spaced H atoms. Fig. 9 shows that the atomic H 1*s* level is broadened into an energy band in the solid. Since there is one electron per H atom and this band can accommodate two altogether, the band is half-filled with paired electrons. The total electronic energy is reduced if the H–H distances alternate since the band splits into two and the higher energy electrons move to lower energy. Eventually, if the distortion proceeds far enough, all the electrons of the infinite chain finish up in H–H σ-bonding orbitals.

A more complex variant of this state-of-affairs is found for the $TiO_2 \rightarrow MoO_2$ distortion. The orbitals with the largest interaction (σ- and π-type) have the largest splittings. Approximately, VO_2 (d^1) has a configuration which fills the lower σ-band, and MoO_2 (d^2) one which fills both lower σ- and π-bands. There is some population of the δ-band in ReO_2 (d^3). All these examples are found in the distorted structure, at least at

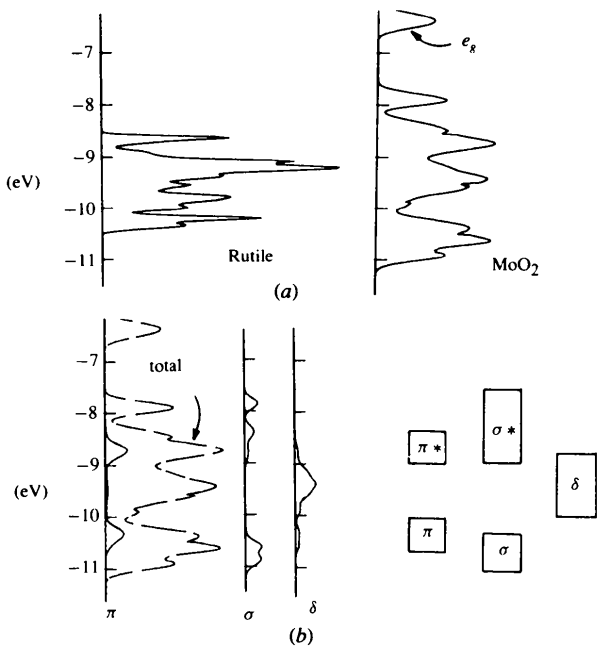

Fig. 11. (*a*) Change in the calculated density-of-states during the distortion $TiO_2 \longrightarrow MoO_2$. (*b*) The decomposition of the total density of states into σ-, π- and δ-components with respect to the edge-sharing chains.

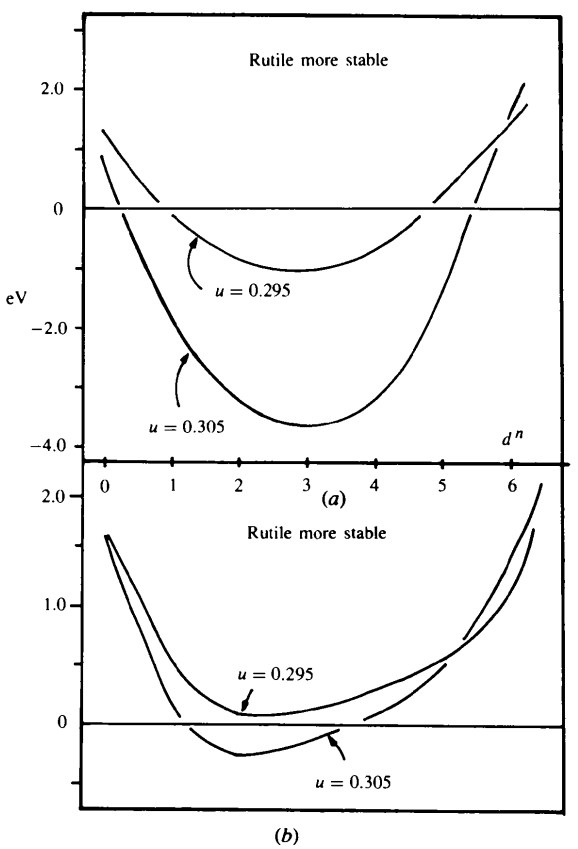

Fig. 12. Calculated difference in energy between the TiO_2 and MoO_2 structures. (*a*) Using the same Ti–O distance of 1.95 Å but two different values of *u*. (*b*) The same as (*a*) but using Fe parameters.

low enough temperature (<340 K for VO_2). We can calculate the energy difference between the two structures as a function of electron count. The results of calculations on TiO_2 (d^0) itself are shown in Fig. 12 (Burdett, 1985). Note that the d^0 configuration is resistant to distortion, as observed for rutile. These are calculations of the 'rigid-band' type. The energy differences for other d counts are obtained by adding (as in this case) or removing electrons to the energy bands resulting from calculations on a single pair of structures with the TiO_2 (d^0) stoichiometry. No change is made in orbital or geometry parameters to mimic different metal atoms. Thus, the general sense of the picture will be correct, but finer details may be missed. Indeed, this rigid-band calculation gives the wrong result for RuO_2 (d^4). This is metallic and has the undistorted rutile structure. The sensitivity of the plots to differences in u parameters and whether orbital parameters for Fe or Ti are used are shown for comparison. Along with the discussion arising from the projected or partial densities of states of Fig. 11(*b*), the general shape of the energy difference curve as a function of d count identifies the driving force for the distortion of stronger metal–metal bonds.

Jahn–Teller distortions in the t_{2g} block

We noted earlier in Table 2 the failure of the local model to account for the distortion modes of systems where there is an asymmetric occupation of the t_{2g} levels. Fig. 13 shows the results (Burdett, Miller, Richardson & Smith, 1985) of a set of calculations using the band model as a function of d count. Notice how different the results are from those of Fig. 7 using the local model. The predictions of this 'extended' model are shown in Table 2. The agreement in terms of the sense of the distortion (**1** or **2**) with experiment is perfect. What is the essential difference between the two sets of calculations?

Of course, from Figs. 10 and 11 we know that metal–metal interactions are important. These are certainly ignored in the local model, irrespective of whether the Crystal Field Theory or an orbital model is used. Also included in the band model and ignored by the local model are the extended interactions between metal centers, coupled by the bridging atom orbitals. We noted the width of the t_{2g} band in several places above. These

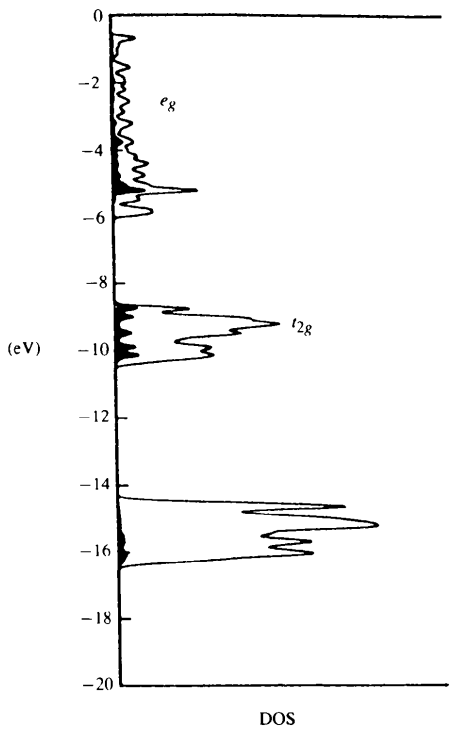

Fig. 14. The contribution of the metal z^2 orbital to the band structure (shaded curve). Notice that contributions appear in both 'e_g' and 't_{2g}' bands. For TiO_2, all bands below 14 eV are filled.

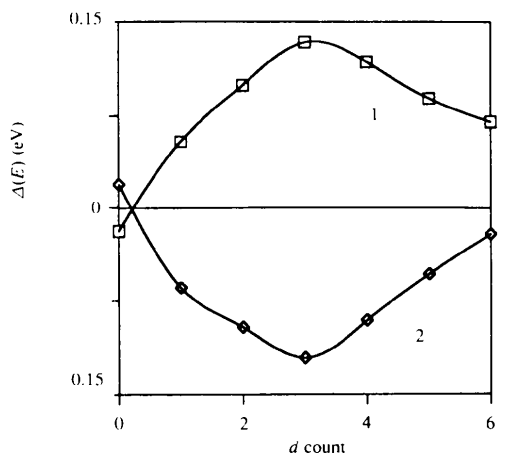

Fig. 13. The stabilization energy on distortion away from octahedral for the two long–four short (**1**) or two short–four long (**2**) pathway for low-spin systems d^0–d^6, using the numerical results of a band model, *cf.* Fig. 7.

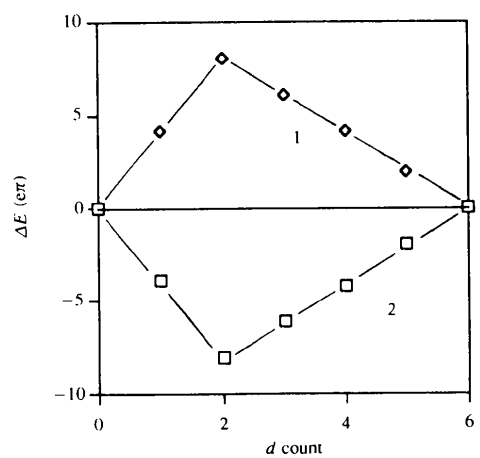

Fig. 15. The stabilization energy on distortion away from octahedral for the two long–four short (**1**) or two short–four long (**2**) pathway for the low-spin systems d^0–d^6 using the Angular Overlap implementation of the band model, *cf.* Fig. 13.

important *M–M* and *M–O* interactions determine its magnitude. One of the important results of the extended coupling which comes naturally from the band model is that the e_g and t_{2g} levels of the *isolated* octahedron do not remain orthogonal but mix together in the extended structure. Fig. 14 shows the contribution of the z^2 orbital to the band structure (Burdett, Miller, Richardson & Smith, 1985). Notice that contributions appear in both 'e_g' and 't_{2g}' bands. On the local model z^2 character should only appear in the e_g band. It is possible to generate the band structure by using the modern orbital analog of Crystal Field Theory, namely The Angular Overlap Model (Burdett, 1980) where such effects are included naturally. The resulting plot to compare with that of Fig. 13 is shown in Fig. 15. The correlation is very striking. At d^0 (TiO_2), no distortion is predicted at all; there are no *d* electrons.

In a nutshell, therefore, although we could discuss this further, the reason for the distortions of systems of this type lies in the extended nature of the interactions. This is perhaps a surprise for the fluorides, systems which certainly are frequently described as largely ionic materials. Notice from Table 2 that when local and extended pictures give the same prediction, the distortion (for FeF_2) is largest. Although the band model gives the correct result for TiO_2 itself, the discussions in this section are not applicable since there are no *d* electrons for this system.

The case of rutile itself

As noted above, the electronic picture for TiO_2 itself must involve orbitals other than the largely metal-located ones discussed, namely the behavior of the largely oxygen *p* band. Two interactions are important, both oxygen–oxygen and metal–oxygen. We noted earlier the importance of metal–oxygen π-bonding. It shows up strongly in Fig. 10(*b*) and will feature again later. One useful way of determining the sense of distortion of a ligand sphere around a central atom where bond length equality is not forced by symmetry is to compare the bond overlap populations for the system where the interatomic separations are set equal. A simple molecular case is shown in Fig. 16(*a*) for the SF_4 molecule (Burdett, 1980). The bond overlap populations are shown from a calculation with equal S–F distances. The 'axial' distances have the smaller population implying longer axial bonds in the real structure, as indeed is found experimentally [Fig. 16(*b*)]. Results of such a calculation (Burdett, Hughbanks, Miller, Richardson & Smith, 1984) on solid TiO_2 are shown in Fig. 16(*c*). The prediction here is thus a distortion of type (**2**), the arrangement which is not found. This is, however, the distortion found in MgF_2.

Evidence that it is the O–O and not the Ti–O interactions which are important is found from the details of diffraction studies at room and low temperatures (Burdett, Hughbanks, Miller, Richardson & Smith, 1984). Table 3 shows the thermal motion parameters at two temperatures. Notice that at room temperature the parameters for oxygen and for titanium are similar. This is unusual. The most common observation is that the heavier atom moves less than the lighter one (the situation found for CrO_2, for example). This is true at low temperature for rutile. Thus, a model for the structure from these results is that the details of the local coordination are set by anion–anion repulsions and that the Ti atom actually rattles a bit in the structure. Fig. 17 shows the results of a band calculation performed on the oxide ions alone. The dimensions of the unit cell were fixed and calculations performed at five different values of the *u* parameter which determines the oxygen positions. A value of $u = 0.303$ defines a regular octahedron. Smaller values correspond to distortion (**2**)

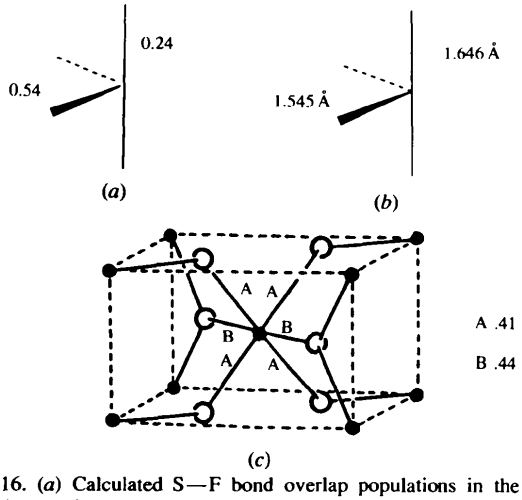

Fig. 16. (*a*) Calculated S—F bond overlap populations in the SF_4 molecule; (*b*) the S—F distances in SF_4; (*c*) calculated Ti—O bond overlap populations in solid TiO_2.

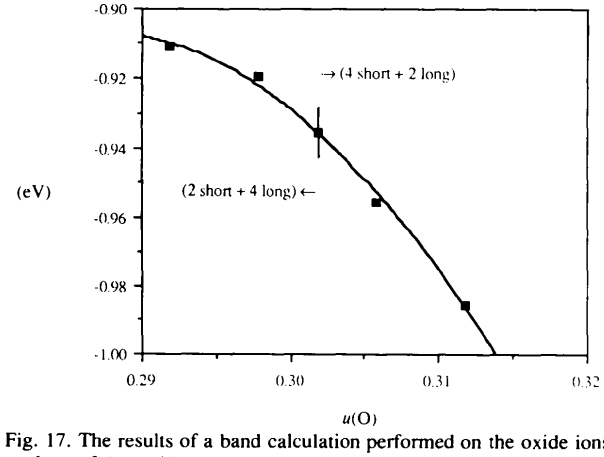

Fig. 17. The results of a band calculation performed on the oxide ions alone of the rutile structure. A value of $u = 0.303$ defines a regular octahedron. Smaller values correspond to distortion (**2**) and larger values to distortion (**1**). The results indicate that distortion (**1**) is energetically favored.

Table 3. *Atomic positions and anisotropic displacement parameters* ($\times 10^3$) *of rutile*

		295 K	15 K
Ti	$x = y = z$	0	0
	$U_{11} = U_{22}$	5.5 (2)	1.2 (2)
	U_{33}	4.5 (3)	1.1 (2)
	U_{12}	−0.3 (3)	−0.2 (2)
	$U_{13} = U_{23}$	0	0
O	$x = y$	0.30476 (6)	0.30469 (6)
	z	0	0
	$U_{11} = U_{22}$	5.7 (1)	3.1 (1)
	U_{33}	4.4 (1)	2.6 (1)
	U_{12}	−1.9 (1)	−0.9 (1)
	$U_{13} = U_{23}$	0	0

The general form for the temperature factor is $\exp[-2\pi^2(U_{11}h^2a^{*2} + \ldots + 2U_{23}klb^*c^*)]$.

and larger values to distortion (**1**). The calculations indeed show the energetic propensity for the oxide substructure to distort in the sense of (**1**). A similar prediction concerning the sense of the distortion comes from a molecular mechanics calculation (Burdett, Hughbanks, Miller, Richardson & Smith, 1984) using (**3**) on the oxide substructure alone. An interesting result is, however, found for MgF_2. With the smaller F^- ion and longer Mg—F distances, this effect is not dominant in this material. It has a distortion of type (**2**).

More about the Jahn–Teller effect in d^9 systems

The structures of both d^9 CuF_2 and h.s. d^4 CrF_2 are significantly distorted away from the 'ideal' rutile structure (Fig. 4). A similar picture holds for the other halides which adopt the cadmium halide structure. The two long–four short distortion is invariably found in systems with these electronic configurations, if all the ligands around the metal are identical. We need to search beyond the simple picture of Fig. 6 to show why distortion (**1**) is favored over (**2**) for these examples. The situation is the opposite for d^{10} examples. Cadmium halide-based mercuric chloride and bromide show a shortening of two *trans* linkages (**2**). In $HgCl_2$ this is so pronounced that the structure consists of linear $HgCl_2$ units packed together and the structure lies far from that of cadmium halide. Linear two-coordination is a structural feature of this electron count. It is found in cuprite (Cu_2O), for example. Hybridization between *nd* and $(n+1)s$ orbitals has long been used (Dunitz & Orgel, 1960) to understand such distortions for d^{10}.

To understand these observations we need to develop (Burdett & Eisenstein, 1992) some of the details of the Jahn–Teller approach. (4) expands the electronic energy, $E_0(q)$, for the electronic ground state $|0>$ as a function of some distortion coordinate q, using the familiar language of perturbation theory (Bartell, 1968). The stability of some (usually high symmetry) structure is tested, initially in first order and then in second order if two pathways are of equal energy in first order or if $E_0^{(1)}(q) = 0$.

$$E_0(q) = E_0^{(0)}(0) + E_1^{(1)}(q) + E_0^{(2)}(q) + \ldots$$
$$= E_0^{(0)}(0) + \langle 0|\partial H/\partial q|0\rangle q + (1/2)[\langle 0|\partial^2 H/\partial q^2|0\rangle - 2\sum_j{}' |\langle 0|\partial H/\partial q|j\rangle|^2/(E_j(0) - E_0(0))]q^2 + \ldots \quad (4)$$

From symmetry arguments, Γ_q, the symmetry species of q, must be contained within the symmetric direct product of Γ_0 for a nonzero value of the first-order term $E_0^{(1)}(q) = \langle 0|\partial H/\partial q|0\rangle$. This leads directly to the first-order Jahn–Teller result that molecules with orbitally degenerate electronic states will distort so as to remove the degeneracy. The electronic ground state of an octahedral d^9 e_g^3 system (Cu^{II}) is ^2E_g. The symmetry species of the distortion coordinate q also follows from symmetry. In this case, q is of e_g symmetry *via* this first-order effect. The electronic ground state of an octahedral Hg^{II} (d^{10}) system is $^1A_{1g}$, which means that the first-order term is identically zero. This system is thus first-order Jahn–Teller inactive.

The first-order result for Cu^{II} tells us that the geometry will distort away from octahedral. It even tells us the symmetry species of the distortion coordinate (e_g). There are, however, an infinite number of choices available for such a degenerate mode. Two are shown in (**6**) and (**7**) (Fig. 18) and we know from quantum mechanics that any linear combination of them is a legitimate motion too. We need to discover why of all these possibilities, it is distortion (**1**) which is found for Cu^{II}. Imposition of a crystal potential which forces (**1**) was an *ad hoc* solution for many years, but the most satisfying route is examination of higher-order terms in (**4**). Consideration of the terms in q^2 of (**4**) leads to the second-order Jahn–Teller effect. The second-order energy term, $E_0^{(2)}(q)$, consists of two parts. The first is $\langle 0|\partial^2 H/\partial q^2|0\rangle$, which may be regarded as the classical force constant which describes the motion of the nuclei in the electronic state $|0\rangle$, one with a frozen electronic charge distribution characteristic of the undistorted ($q = 0$) structure. The second term, $-\sum_j{}' |\langle 0|\partial H/\partial q|j\rangle|^2/(E_j(0) - E_0(0))$, is always negative (*i.e.* stabilizing) and represents the relaxation of this frozen charge distribution on vibration.

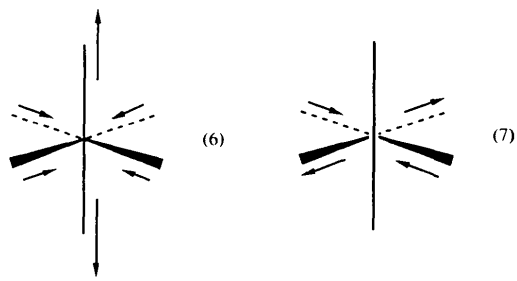

Fig. 18. One possible way of writing the two components of the degenerate Jahn–Teller-active vibrational mode of e_g symmetry. The vibration is doubly degenerate and thus all possible combinations of (**6**) and (**7**) are also possible solutions.

Formally it arises *via* the mixing of excited electronic states into the electronic ground state during the distortion. The sign of $E_0^2(q)$ is determined by the competition between these two terms. The energy gap $E_j(0) - E_0(0)$ in the denominator tells us that this negative contribution will be most important for close-lying electronic states. If one such state, $|j\rangle$, is of the correct symmetry ($\Gamma_q = \Gamma_0 \times \Gamma_j$), the leading term in this expansion can then be large and $E_0^2(q)$ may become negative. The molecule may now distort away from the symmetrical structure along the coordinate q. Since the lowest-lying excited state is usually constructed by removing an electron from the HOMO and placing it in the LUMO, an alternative view of the distortion is one driven by mixing HOMO and LUMO, the HOMO being stabilized as the distortion proceeds. It is that distortion coordinate which allows the two to become of the same symmetry. The state picture of (**4**) may then be reduced to an orbital one, the symmetry species of q being given by $\Gamma_q = \Gamma_{\text{HOMO}} \times \Gamma_{\text{LUMO}}$.

Mixing of nd and $(n+1)s$ orbitals has already been mentioned in connection with Hg^{II} and d^{10} chemistry in general. At the right-hand side of the periodic table, the energy separation between these orbitals is small and thus the energy gap $[E_j(0) - E_0(0)]$ which occurs in $E_0^2(q)$ is also small. In the D_{4h} point group, $(n+1)s$ and nz^2 orbitals are of the same symmetry and thus may mix together during the $O_h \rightarrow D_{4h}$ distortion. The $x^2 - y^2$ orbital is of the wrong symmetry to mix with $(n+1)s$. Fig. 19 shows how these interactions change the picture of Fig. 6, and reveals the power of an orbital model over the Crystal Field Model. Thus, one clearly sees why the two long–four short distortion (**1**) is favored for the d^9 configuration over the two short–four long distortion (**2**). This d–s mixing leads to an electronic energy stabilization of $2\Delta E_1$ for (**1**) and ΔE_2 for (**2**). Assuming that the energy gap $E_j(0) - E_0(0)$ is just the $(n+1)s/z^2$ separation, the stabilization of z^2 will thus be larger in the two short–four long case than for the converse ($|\Delta E_1| < |\Delta E_2|$). As a result, the best electronic stabilization for the d^{10} configuration is for the two short–four long case (**2**), since here nz^2 lies closer to $(n+1)s$. Thus, in a very interesting way, theoretical concepts of use in one part of the periodic table naturally lead to insights in another. Perhaps we should have anticipated this. Distortions of a parent structure (cadmium halide) of opposite type (two long–four short or two short–four long) as a function of electron count (d^9 or d^{10}) should surely be connected somehow.

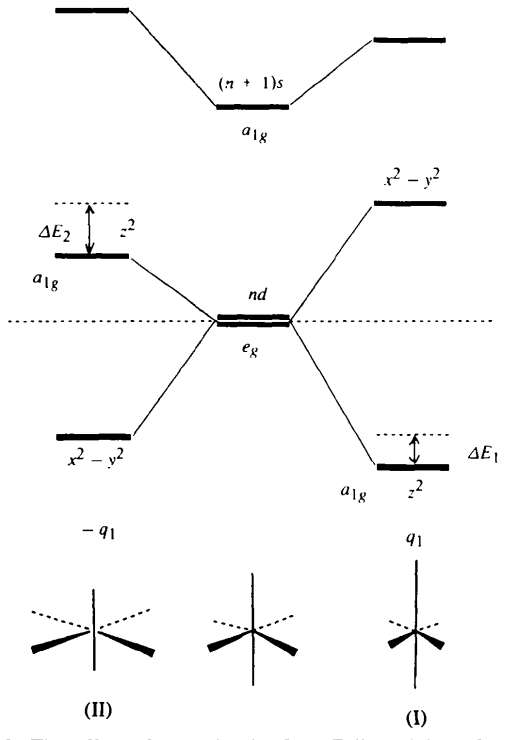

Fig. 19. The effect of second-order Jahn–Teller mixing of nd and $(n+1)s$ orbitals in octahedral systems. From energy-gap arguments, $|\Delta E_1| < |\Delta E_2|$.

The planar anion in rutile

We noted earlier that one of the interesting features of the rutile structure (and indeed of anatase too) is the rigorously planar anion. A suspicion exists that such a geometric feature is associated with the first-row ions of O and F, since MX_2 compounds with chalcogenides or heavier halides adopt a structure such as that of $CdCl_2$ (Fig. 2) where a pyramidal anion is found. (Note, however, that this cannot be the whole story since PtO_2 adopts the $CaCl_2$ structure where the anion is nonplanar.) This viewpoint arises from molecular chemistry where, although $N(CH_3)_3$, $P(CH_3)_3$ and $P(SiH_3)_3$ are pyramidal, $N(SiH_3)_3$ has a planar skeleton. The traditional explanation of this observation is quite simple (Albright, Burdett & Whangbo, 1985, p. 147). The σ-framework of all these molecules energetically prefers a pyramidal geometry, a result accessible using the simplest of theories (*e.g.* ence) is usually quite small (*ca* 21 kj mol^{-1} for NH_3), compared with their heavier analogs (*ca* 147 kj mol^{-1} for ence) is usually quite small (ca 21 kj mol^{-1} for NH_3), compared with their heavier analogs (ca 147 kj mol^{-1} for PH_3). Thus, the energetic consequences of π-bonding may be important in determining angular geometry in such cases. Fig. 20(*a*) shows the interaction between the highest occupied orbital on the σ-framework of some AX_3 unit (a nonbonding orbital on A) wth a π-acceptor orbital on X. The interaction is largest at the planar structure where overlap is largest. Such an interaction thus favors a planar structure. If the σ-inversion barrier is small, as is often the case for A = first-row atom, the π-effect is thus predominant and a planar geometry will be found. The nature of the acceptor orbital depends on the system. For the molecules NH_3 and PH_3, the acceptor orbital of importance is a σ^* SiH_3 level [Fig. 20(*b*)]. For

rutile the corresponding interaction is one of π-type between metal d and oxygen p orbitals, as shown in Fig. 20(c). A similar type of interaction stabilizes (Burdett & Hughbanks, 1984) a square-planar O atom in the structure of NbO [Fig. 20(d)]. The importance of such π-interactions has featured largely in this article. The idea was first introduced in Fig. 9(b).

There is, however, a richer chemistry here than just the stabilization of the planar oxygen. As Fig. 20(a) shows, the stabilization of the planar geometry is associated with occupation of the bonding orbital. Occupation of the antibonding higher-energy orbital of the pair will destabilize the planar geometry. Thus, a planar structure is only expected if there is excess 'π-bonding' over 'π-antibonding' electrons. In the rutile case, bearing in mind the nature of the π-acceptor orbital, certainly by the time the d^6 configuration is reached, all the antibonding levels of this type should be filled. At this point the planar oxygen should be electronically disfavored. Fig. 21 shows the results of a set of calculations comparing the $CaCl_2$ structure (pyramidal anion) with rutile (planar anion). Notice the crossover in stability between d^5 and d^6. The result is in perfect agreement with experiment. Only PtO_2 (d^6) of all the rutile-type oxides adopts the $CaCl_2$ structure (Rogers, Shannon, Sleight & Gilson, 1969). Although we have used an electronic explanation here, O'Keeffe & Hyde (1979) have stressed the importance of nonbonded repulsions (between the oxide ions in this case) in influencing problems of this type.

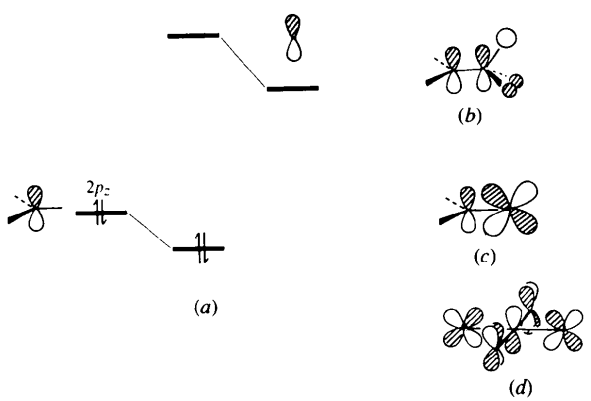

Fig. 20. (a) Stabilization of the oxygen $p\pi$-orbital by an acceptor orbital on a ligand. (b) A σ^* SiH_3 level leading to the planar geometry in $N(SiH_3)_3$. (c) π-type interaction between metal d and oxygen p orbitals in rutile. (d) Stabilization of square-planar oxygen in NbO. In (c) and (d) the types of orbital are identical, but the coordination number is different. The acceptor orbital shown is a p orbital [as in (a)], but it is a d orbital in (b) and (c).

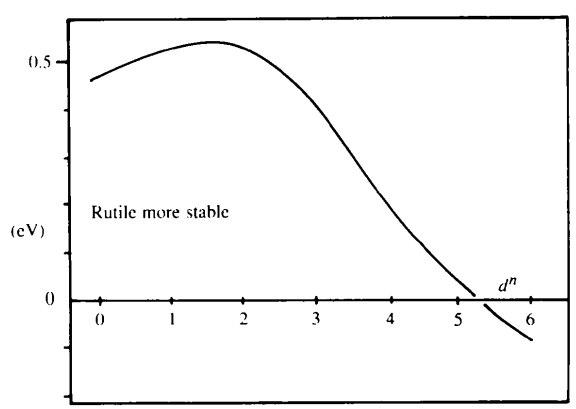

Fig. 21. Calculated energy difference between the $CaCl_2$ and rutile structures as a function of d count. Notice that the $CaCl_2$ structure with its pyramidal anion becomes more stable than the rutile structure with its planar anion for d^6 cations.

Rutile *versus* α-PbO_2

With this final example we examine the stability of another structure geometrically quite similar to that of rutile, the α-PbO_2 structure. This is shown in Fig. 5(b) and consists of a zigzag arrangement of filled octahedral holes of the close-packed structure, rather than the linear arrangement of Fig. 1 found for rutile. A variant containing metal–metal dimers is also known as the β-form of ReO_2. Thus, both systems distort: $TiO_2 \rightarrow MoO_2$ and α-$PbO_2 \rightarrow \beta$-ReO_2. Fig. 22 shows the results (Burdett, 1985) of some rigid band calculations on the two pairs of systems TiO_2, MoO_2 and α-PbO_2, β-ReO_2. Notice the best stability of the zigzag structure at the half-filled d band, which is where β-ReO_2 (d^3) is located. Notice, however, that the calculations overestimate in general the stability of the α-PbO_2 or β-ReO_2 structure. In spite of this we can inquire as to the origin of these curves. A full investigation would involve discussion of the method of moments (Burdett, 1988a, 1995; Lee,

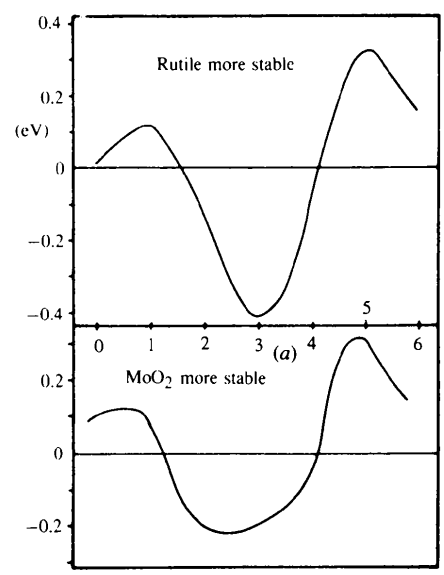

Fig. 22. Calculated energy difference between (a) the TiO_2 (rutile) and α-PbO_2 structures and (b) calculated energy difference between the MoO_2 and β-ReO_2 structures as a function of d count.

1991), but even without this we can make some broad generalizations with the help of the geometry of allene [Fig. 23(*a*)]. For the allene electron count (four π-electrons), the stable geometry is twisted, where there is no conjugation along the chain. For two more or two fewer π-electrons, the planar structure is predicted to be more stable. Thus, the energy difference curve as a function of the number of π-electrons [Fig. 23(*b*)] has the same form as the curves in Fig. 22. The MO diagram of allene is shown in Fig. 23(*a*), and it is easy to see numerically from this diagram why the preferred structural conformation varies with electron count. An exactly analogous explanation lies behind the TiO_2/α-PbO_2 plot. Metal–metal interactions conjugated along the chain [Fig. 24(*a*)] are favored for early and late *d* counts, with the structure where local pairwise bonding occurs [Fig. 24(*b*)] stable at the half-filled point. This is a result discussed in more conventional terms earlier (Rogers, Shannon, Sleight & Gilson, 1969).

Concluding remarks

It should be clear in the set of examples chosen here that there is a mix of 'old theory', which has often not been very helpful, and 'new theory' which has brought many rather different observations together. Such a unifying picture is a satisfying one in the sense that the band model used to study these systems is just the solid-state analog of molecular orbital theory. In fact, we have made use of orbital arguments initially devised for allene, trisilylamine amongst others. During the past decade the delocalized orbital picture has been one that has seen great acceptance by the molecular community. At the same time it has become well used by chemists whose main activity lies in the area of solids. For those of us who wonder at the unity of nature, the use of the same theoretical model in both areas has a particular appeal.

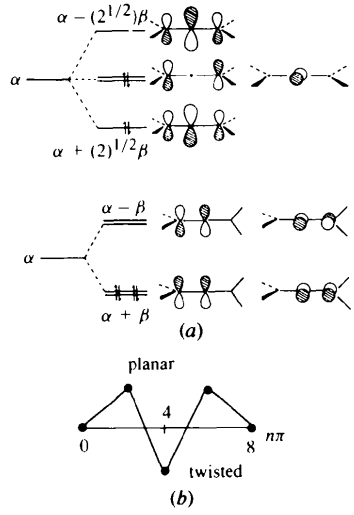

Fig. 23. (*a*) The MO diagrams for allene conformers. (*b*) The energy difference curve between them as a function of the number of π-electrons.

Fig. 24. (*a*) Conjugated π metal–metal interactions along the chain in TiO_2 (rutile). (*b*) Local pairwise interaction in α-PbO_2.

This research has been supported over the years by the National Science Foundation. I would also like to thank my coworkers who worked on rutile, T. Hughbanks, G. J. Miller, J. W. Richardson and J. V. Smith.

References

ALBRIGHT, T. A., BURDETT, J. K. & WHANGBO, M.-H. (1985). *Orbital Interactions in Chemistry*. New York: Wiley.

BARTELL, L. S. (1968). *J. Chem. Educ.* **45**, 754–766.

BAUR, W. H. (1961). *Acta Cryst.* **14**, 209–215.

BAUR, W. H. (1976). *Acta Cryst.* B**32**, 2200–2207.

BAUR, W. H. (1981). *Mater. Res. Bull.* **16**, 339–344.

BAUR, W. H. (1994). *Z. Krist.* **209**, 143–149.

BAUR, W. H. & KHAN, A. A. (1971). *Acta Cryst.* B**27**, 2133–2140.

BURDETT, J. K. (1980). *Molecular Shapes: Theoretical Models of Inorganic Stereochemistry*. New York: Wiley.

BURDETT, J. K. (1984). *Prog. Solid State Chem.* **15**, 173–255.

BURDETT, J. K. (1985). *Inorg. Chem.* **24**, 2244–2253.

BURDETT, J. K. (1988*a*). *Acc. Chem. Res.* **21**, 189–194.

BURDETT, J. K. (1988*b*). *Chem. Rev.* **83**, 3–30.

BURDETT, J. K. (1995). *Chemical Bonding In Solids*. New York: Oxford University Press.

BURDETT, J. K. & EISENSTEIN, O. (1992). *Inorg. Chem.* **31**, 1758–1766.

BURDETT, J. K. & HUGHBANKS, T. (1984). *J. Am. Chem. Soc.* **106**, 3101–3113.

BURDETT, J. K., HUGHBANKS, T., MILLER, G. J., RICHARDSON, J. W. & SMITH, J. V. (1984). *J. Am. Chem. Soc.* **109**, 3639–3646.

BURDETT, J. K., MILLER, G. J., RICHARDSON, J. W. & SMITH, J. V. (1985). *J. Am. Chem. Soc.* **110**, 8064–8071.

BURDETT, J. K., PRICE, S. L. & PRICE, G. D. (1981). *Solid State Commun.* **40**, 923–926.

CATLOW, C. R. A. & MACKRODT, W. C. (1982). Editors. *Computer Simulation of Solids*. Berlin: Springer-Verlag.

COHEN, M. L. (1981). In *Structure and Bonding in Crystals*, edited by M. O'KEEFFE & A. NAVROTSKY, Vol. 1. New York: Academic Press.

DUNITZ, J. D. & ORGEL, L. E. (1960). *Adv. Inorg. Chem. Radiochem.* **2**, 1–48.

DUNN, T. M., MCCLURE, D. S. & PEARSON, R. G. (1965). *Some Aspects of Crystal Field Theory*. New York: Harper and Row.

EVANS, R. C. (1964). *An Introduction to Crystal Chemistry*, 2nd ed. Cambridge Univ. Press.

GOODENOUGH, J. B. (1965). *Bull. Soc. Chim. Fr.* **4**, 1200–1204.

HOFFMANN, R. (1988). *Solids and Surfaces*. New York: VCH Publishers.

JAHN, H. A. & TELLER, E. (1937). *Proc. R. Soc. A*, **161**, 220–232.

LEE, S. (1991). *Acc. Chem. Res.* **24**, 249–255.

O'KEEFFE, M. (1977). *Acta Cryst.* A**33**, 924–930.

O'KEEFFE, M. & HYDE, B. G. (1979). *Trans. Am. Crystallogr. Assoc.* **15**, 65–69.

PAULING, L. (1929). *J. Am. Chem. Soc.* **51**, 1010–1031.

PEIERLS, R. E. (1955). *Quantum Theory of Solids*. Oxford Univ. Press.

ROGERS, D. B., SHANNON, R. D., SLEIGHT, A. W. & GILSON, J. L. (1969). *Inorg. Chem.* **8**, 841–847.

ZUNGER, A. (1981). In *Structure and Bonding in Crystals*, edited by M. O'KEEFFE & A. NAVROTSKY. Vol. 1. New York: Academic Press.